Hydrodynamic Heat Transport Regime in Bismuth: A Theoretical Viewpoint

Maxime Markov,[1,*] Jelena Sjakste,[1] Giuliana Barbarino,[1] Giorgia Fugallo,[2] Lorenzo Paulatto,[3] Michele Lazzeri,[3] Francesco Mauri,[4] and Nathalie Vast[1]

[1]*École Polytechnique, Laboratoire des Solides Irradiés, CNRS UMR 7642, CEA-DSM-IRAMIS, Université Paris-Saclay, F91128 Palaiseau cédex, France*

[2]*CNRS, LTN UMR 6607, PolytechNantes, Université de Nantes, Rue Christian Pauc, 44306 Nantes cédex 3, France*

[3]*Sorbonne Universités, UPMC Université Paris 06, CNRS UMR 7590, MNHN, IRD UMR 206 Institut de Minéralogie, de Physique des Matériaux et de Cosmochimie, 75005 Paris, France*

[4]*Dipartimento di Fisica, Università di Roma La Sapienza, Piazzale Aldo Moro 5, I-00185 Roma, Italy*

(Received 9 May 2017; published 14 February 2018)

Bismuth is one of the rare materials in which second sound has been experimentally observed. Our exact calculations of thermal transport with the Boltzmann equation predict the occurrence of this Poiseuille phonon flow between ≈1.5 and ≈3.5 K, in a sample size of 3.86 and 9.06 mm, consistent with the experimental observations. Hydrodynamic heat flow characteristics are given for any temperature: heat wave propagation length, drift velocity, and Knudsen number. We discuss a gedanken experiment allowing us to assess the presence of a hydrodynamic regime in any bulk material.

DOI: 10.1103/PhysRevLett.120.075901

Currently, a lot of attention is devoted to the study of phonon-based heat transport regimes in nanostructures [1–4]. Of particular interest is the hydrodynamic regime, in which a number of fascinating phenomena such as Poiseuille's phonon flow and second sound occur and where temperature fluctuations are predicted to propagate as a true temperature wave of the form $e^{i(\mathbf{k}\cdot\mathbf{r}-\omega t)}$ [5]. The theoretical study of the hydrodynamic regime has encountered a renewed interest in graphene nanoribbons, where the breakdown of the diffusive Fourier law in favor of the second sound propagation has been predicted [6–9]. Bismuth is a semimetal with relatively low carrier concentrations so that the dominant mechanism for heat conduction at low temperatures is via phonons [10,11]. Together with solid helium [12] and NaF [13], it is one of the rare materials that is sufficiently isotopically pure so that second sound could be observed. Physical and chemical perfection of Bi crystals is so high that also "transitions" between the various regimes have been experimentally observed with the increase of the (yet cryogenic) temperature: from heat transport via ballistic phonons, to the regime of Poiseuille's flow with second sound, to the diffusive (Fourier) propagation [10].

Neither the conditions for the occurrence of the hydrodynamic regime nor the transition temperatures have ever been supported by a theoretical work in one of the above-cited 3D materials. So far, phonon hydrodynamics has been studied with the lattice Boltzmann formalism for a model dielectric material with an *ad hoc* three-phonon collision term and no resistive processes [14]. The transition to the kinetic regime has been modeled in group IV semiconductors through a hydrodynamic-to-kinetic switching factor proportional to the ratio of normal and resistive scattering rates [15–17]. A review of advances in phonon hydrodynamics points out the lack of a widely applicable hydrodynamic model that would consider all of the normal and resistive processes [5].

In this Letter, a major advance consists of accounting for the phonon repopulation by the normal processes in the framework of the exact variational solution of the Boltzmann transport equation (V-BTE) [18,19], coupled to the *ab initio* description of anharmonicity: three-phonon collisions turn out to be particularly strong at low temperatures and lead to the creation of new phonons in the direction of the heat flow (normal processes), which enhance the heat transport. This induces time and length scales over which heat carriers behave collectively and form a hydrodynamic flow that cannot be described by independent phonons with their own energy and lifetime. In other words, the single mode approximation (SMA), valid for the phonon gas model, breaks down. The resistive processes are entirely controlled by few phonon-phonon anharmonic processes, which lead to the creation of phonons in the direction opposite to the heat flow (umklapp processes), and by extrinsic processes coming from phonon scattering by the sample boundaries.

The characterization of heat transport regimes, and, in particular, of the transition between the hydrodynamic and kinetic regimes, is the main focus of the present Letter. We discuss several methods to define the hydrodynamic regime and provide the link with macroscopic scale quantities [5], like Knudsen number and drift velocity. In particular, we extract the heat wave propagation length (HWPL) directly from the lattice thermal conductivity (LTC) calculated with

V-BTE. We argue that our method to extract the HWPL from the LTC in samples of different sizes, combined with a measurement of the average phonon mean free path, can be viewed as a gedanken experiment that could allow us to determine the transition from the hydrodynamic-to-kinetic regime in any material.

Several criteria are used in order to identify the hydrodynamic-to-kinetic transition. First, the picture of the heat carried by single (uncorrelated) phonons with finite lifetimes is valid in the kinetic regime only. Thus, a significant difference between the LTC obtained by a solution of V-BTE and the one obtained in the single mode approximation (SMA-BTE) is the indication that the hydrodynamic regime is achieved. Second, we compare the thermodynamic averages of the phonon-scattering rates for normal and resistive processes Γ^n and Γ^U, and the hydrodynamic regime occurs when [20]

$$\Gamma^U_{\mathrm{av}} \ll \Gamma^n_{\mathrm{av}}. \tag{1}$$

Then, we address the question of the occurrence of Poiseuille's flow inside the hydrodynamic regime. Here as well, various methods are employed, which now account for the additional scattering rate by sample boundaries Γ^b. We first use Guyer's conditions [20],

$$\Gamma^U_{\mathrm{av}} < \Gamma^b_{\mathrm{av}} < \Gamma^n_{\mathrm{av}} \tag{2}$$

and find the temperature interval in which second sound is calculated to be observable. In the second method, we extract the HWPL directly from the LTC calculated with V-BTE and compare it to the sample size, which sets the threshold for the second sound observability. Above the threshold, the heat wave is damped before reaching the sample boundary.

The thermodynamic averages of phonon-scattering rates for normal, umklapp, and boundary collisional processes that condition the transport regime read

$$\Gamma^i_{\mathrm{av}} = \frac{\sum_\nu C_\nu \Gamma^i_\nu}{\sum_\nu C_\nu} \tag{3}$$

where C_ν is the specific heat (see below) of the phonon mode $\nu = \{\mathbf{q}j\}$ and the index $i = n$, U, b stands for normal, umklapp, and extrinsic (boundary) scattering, respectively. Besides the scattering rate (or inverse relaxation time), the quantities characterizing heat transport are the drift velocity v of the heat carriers defined below and the phonon propagation length $\lambda = v\Gamma^{-1}_{\mathrm{av}}$, which is the characteristic distance that heat carrying phonons cover before damping. As a source of damping, we consider, in infinite samples, either umklapp processes only,

$$\lambda_{\mathrm{hydro}}(\infty) = v/\Gamma^U_{\mathrm{av}}, \tag{4}$$

or their combination with normal processes through Matthiessen's rule,

$$\lambda_{\mathrm{gas}}(\infty) = v/(\Gamma^U_{\mathrm{av}} + \Gamma^n_{\mathrm{av}}). \tag{5}$$

When scattering by sample boundaries is accounted for, the phonon propagation length reads $\lambda(L^{\mathrm{Cas}})$ instead of $\lambda(\infty)$ in Eqs. (4) and (5), where Casimir's length L^{Cas} represents the smallest dimension of the sample or nanostructure.

In bismuth, the transport is anisotropic and has components along the trigonal axis ($\parallel$) and perpendicular ($\perp$) to it, i.e., along the binary and bisectrix directions. The drift velocity in these directions reads [9]

$$v_j^2 = \frac{\sum_\nu C_\nu \mathbf{c}_{\nu j} \cdot \mathbf{c}_{\nu j}}{\sum_\nu C_\nu}, \tag{6}$$

where j stands for the $\parallel$ or $\perp$ direction and $\mathbf{c}_\nu$ is the phonon group velocity. In the thermodynamic averages, the specific heat of a phonon mode is calculated as $C_\nu = n^0_\nu(n^0_\nu + 1)[(\hbar\omega_\nu)^2/k_B T^2]$, where n^0 stands for the temperature (T)-dependent Bose-Einstein phonon occupation number and ω_ν is the phonon frequency.

The LTC, third-order anharmonic constants of the normal and umklapp phonon interactions, and thermodynamical averages have been calculated on a $28 \times 28 \times 28$ $\mathbf{q}$-point grid in the Brillouin zone, but for the drift velocity below 2 K, which required a $40 \times 40 \times 40$ grid. Details of the calculation are given in the Supplemental Material [21]. We have used the wire geometry for boundary scattering with Casimir's model, $\Gamma^b = [n^0_\nu(n^0_\nu + 1)|\mathbf{c}^b_\nu|/FL^{\mathrm{Cas}}]$, where $\mathbf{c}^b_\nu$ is the group velocity in the direction of the smallest dimension. Specularity [24–26] is neglected and $(1/F)$ accounts for the geometrical ratio of L^{Cas} over the finite (yet large) dimension along the heat transport direction [19,21,27–29]. Varying $(1/F)$ by 2 ± 1 (Fig. 1) has little consequence on $\kappa_\perp$ above $T = 2$ K.

Remarkably, our calculated LTC shows the same evolution as the experimental one over 3 orders of magnitude (Fig. 1, respectively, black dotted and green dashed lines), and the various regimes of heat transport are excellently described from ambient temperature down to 2 K. The LTC increases as T^{-1} with the decrease of temperature down to 10 K. Then, in the absence of scattering other than phonon-phonon interaction, the LTC shows an exponential growth below 10 K (black solid line). This behavior is directly due to the weakness of resistive (umklapp) processes.

The account for boundary scattering makes the LTC value remain finite even in the asymptotic limit. Moreover, the theoretical curves satisfactorily explain the experimental behavior of the LTC and, in particular, the position of the conductivity maximum $T^{\max}$, which is found to be 3.2 K for the 9.72 mm wire, in extremely satisfactory agreement with the maximum at 3.6 K observed in experiment (Fig. 1, respectively, black dotted and green dashed lines). Further

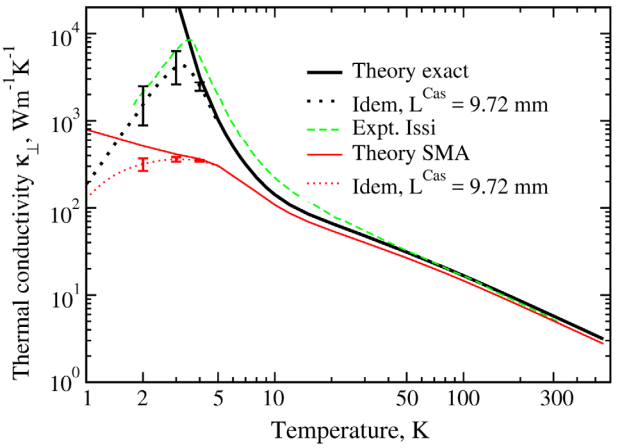

FIG. 1. Temperature dependence of the LTC in the binary direction for a single crystal without (solid lines) or with (dotted lines) millimeter-sized sample boundaries (MSSB). Black curves: Exact variational calculation (V-BTE). Single mode approximation (SMA-BTE), (Red curves). MSSB modeled with the wire geometry and $L^{\mathrm{Cas}} = 9.72$ mm [30]. LTC extracted by us from experiment of Ref. [31] for $T > 20$ K (Green dashed lines); for $T < 20$ K, LTC from a sample having a rectangular cross section 8.8×8.6 mm^2 (Ref. [11]). We used the T-independent bulk value of 6 W(Km)$^{-1}$ [27,28] of the electronic contribution to extract the LTC from the total thermal conductivity of Bi [11]. The error bar in our calculations results from the variation of the geometrical factor $(1/F) = 2 \pm 1$.

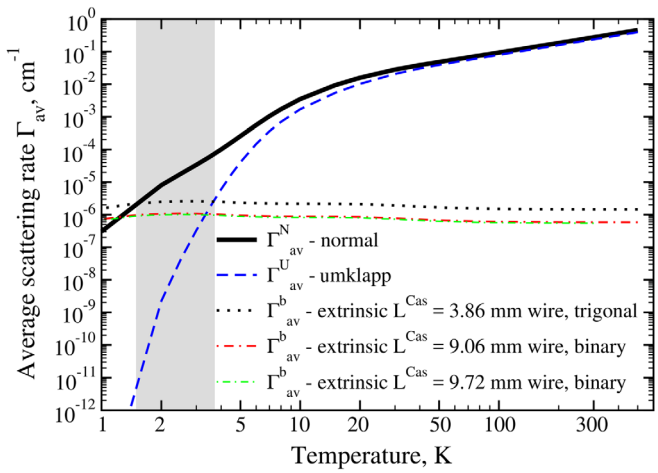

FIG. 2. Temperature dependence of the thermodynamic average of the anharmonic scattering rates for normal and umklapp processes (respectively, black solid and blue dashed line) and of the (boundary) extrinsic scattering rates (ESRs) (dashed black, dot-dashed red and green lines). ESRs have been calculated for a wire geometry using $L^{\mathrm{Cas}} = 3.86$ [32] and $L^{\mathrm{Cas}} = 9.06$ mm [33], and with $L^{\mathrm{Cas}} = 9.72$ mm [30] as in Fig 1. ESRs for $L^{\mathrm{Cas}} = 9.06$ and $L^{\mathrm{Cas}} = 9.72$ mm are hardly distinguishable on the scale of the figure. The shaded region corresponds to the temperature interval in which a second sound peak has been reported, $1.5 < T < 3.5$ K for a length of 3.86 mm in the trigonal propagation direction [10].

decrease of temperature leads to a decrease of the LTC with a decay law gradually approaching the T^3 behavior expected for a regime in which boundary scattering dominates.

The first sign of the transition from the kinetic to hydrodynamic regime around 3 K in infinite samples is demonstrated in Fig. 1 by a large ($> 10^2$) difference between our V- and SMA-BTE results for the LTC (respectively, black and red solid lines). This result shows that the repopulation of phonon states due to normal processes plays an important role, invalidating the SMA picture in which individual phonons have lifetimes and propagation lengths determined by all of the collisional processes [normal and umklapp, Eq. (5)]. The same conclusion can be drawn by considering Fig. 2, where, around 3 K, normal processes dominate over the resistive ones (umklapp) by more than one order of magnitude, so that Eq. (1) is fulfilled.

The same difference in the LTC between V- and SMA-BTE is found in the presence of sample boundaries (Fig. 1, respectively, black and red dotted lines) and, remarkably, the average extrinsic scattering rate Γ^b_{av} calculated with Casimir's length $L^{\mathrm{Cas}} = 3.86$ mm (Fig. 2, black dotted line) lays in between the average normal Γ^n_{av} and umklapp Γ^U_{av} scattering rates and thus satisfy the criterion of Eq. (2) for the existence of Poiseuille's flow and second sound observability [20]. The temperature interval calculated with Eq. (2) is $1.5 < T < 3.6$ K, in perfect agreement with the temperature range $1.5 < T < 3.5$ K, in which second sound has been observed experimentally in the trigonal direction (gray shaded region) [10]. For $L^{\mathrm{Cas}} = 9.06$ mm in the binary direction (red dot-dashed line), the calculated interval is $1.3 < T < 3.4$ K, a temperature range slightly more extended than the experimental one, $3.0 < T < 3.48$ K [10]. In our calculations, Poiseuille's regime ends for temperatures lower than 1.5 K, where phonon scattering by sample boundaries becomes significant (Fig. 2).

However, the average scattering rates discussed so far do not contain any information about repopulation mechanisms [34]. To account for them, we extract a heat wave propagation length L_h that we define by the criterion

$$\kappa(T, L^{\mathrm{Cas}} = L_h) = \kappa(T, \infty)/e, \tag{7}$$

where $\kappa(T, \infty)$ denotes the LTC obtained for an infinite sample at a given temperature, and $\kappa(T, L^{\mathrm{Cas}})$ denotes the LTC obtained for a sample of finite dimension. The extracted HWPL L_h is the cylindrical wire diameter L^{Cas} needed to reduce $\kappa(T, \infty)$ by e (Fig. 3, filled disks, and Supplemental Material for the trigonal direction [36]).

Remarkably, at low temperatures, L_h is found to be close to the phonon propagation length computed with umklapp processes only [Eq. (4)]. These resistive processes damp the heat wave, thus defining the wave traveling distance between the instant of heat wave generation to complete diffusion.

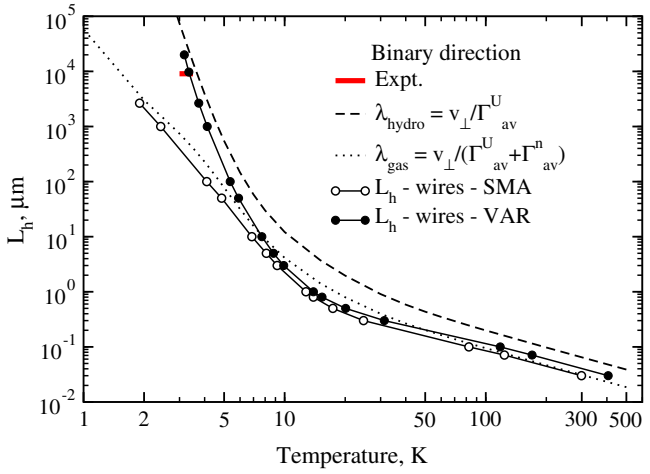

FIG. 3. Heat wave propagation length $L_h(T)$ extracted from the LTC calculations in the binary direction. L_h obtained with V-BTE, accounting for phonon repopulation, (Solid line with black filled disks). L_h obtained with SMA-BTE, (Solid line with empty circles). Phonon propagation length λ_{hydro} of Eq. (4), (Black dashed line). Phonon propagation length λ_{gas} of Eq. (5), (Black dotted line). The red line segment marks the ranges of temperatures, from 3.0 to 3.48 K, and sample dimension, 9.06 mm, in which a second sound peak has been reported in the binary direction [10].

A strong presence of normal processes, in turn, favors heat conduction and second sound behavior. With the increase of temperature, L_h becomes close to the phonon propagation length, accounting for both umklapp and normal processes of Eq. (5), i.e., of an uncorrelated phonon gas (empty circles). We see that the behavior of L_h as a function of temperature is the fingerprint of the transition from the hydrodynamic-to-kinetic regime. The temperature range and sample dimension in which observations of second sound are available in the binary direction (red line segment) are in extremely satisfactory agreement with the calculations, which support the occurrence of second sound at 3.0 K for a 9.72 mm wire. Figure 3 enables us also to predict the occurrence of second sound at other temperatures and sample sizes, for instance, at 4.1 K in a 1 mm size wire.

We emphasize that L_h is a measurable quantity, provided that LTC can be measured in samples of many different sizes, including very large ones. In that sense, the results presented in Fig. 3 can be viewed as a gedanken experiment in which (i) first, one needs to determine the heat wave propagation length from the thermal conductivity measured in samples of different sizes, as described with Eq. (7), and (ii) second, its combination with a measurement of the average phonon mean free path in a bulk sample, given by Eq. (5), as done, for example, in attenuation measurement experiments [39], could, in principle, lead to the identification of the temperature and sample size ranges in which Poiseuille's flow occurs.

We turn to the characterization of Poiseuille's flow, defined above as the range of temperatures and propagation

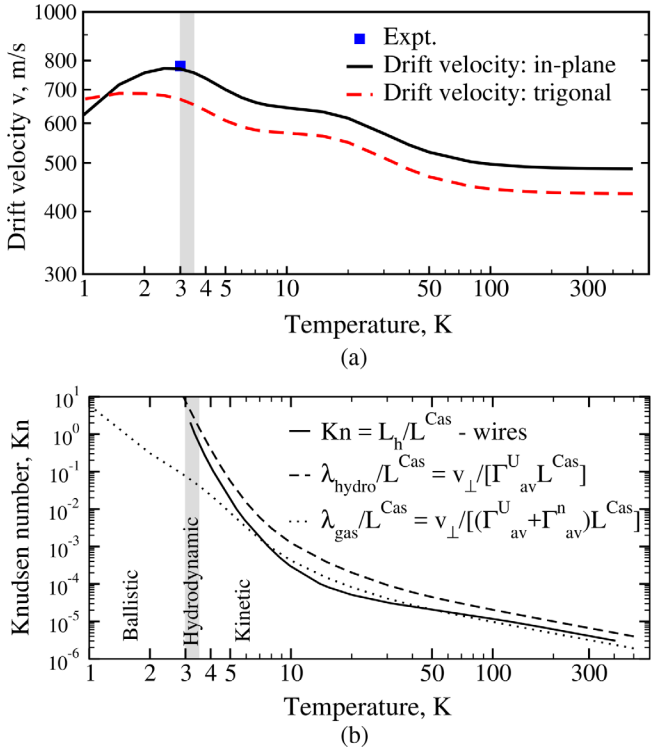

FIG. 4. Heat flow characteristics in Bi as a function of T. (a) Drift velocity v in the binary ($\perp$) and trigonal ($\parallel$) directions (respectively, black solid and red dashed lines). Saturated second sound velocity measured at 3 K [10], (Symbol). (b) Knudsen number for a wire of Casimir's length $L^{\text{Cas}} = 9.72$ mm (black solid line). The ratio of the phonon propagation length in the hydrodynamic (gas) regime over L^{Cas} is given by the dashed (dotted) line. The shaded region $3.0 < T < 3.48$ K corresponds to the interval in which second sound has been observed in the binary direction [10].

lengths where L_h and λ_{hydro} are close to each other. For this purpose, we use common hydrodynamic quantities: Knudsen number (Kn) and drift velocity. The former is defined as the ratio between the HWPL and the characteristic dimension of transport,

$$\text{Kn} = \frac{L_h}{L^{\text{Cas}}}. \tag{8}$$

Interestingly, the transition between the hydrodynamic and kinetic regime is found for a calculated Knudsen number $\text{Kn} \approx 0.58$ at $T = 3.5$ K in agreement with the criteria of phonon hydrodynamics $0.1 \lesssim \text{Kn} \lesssim 10$ [5] (Fig. 4, bottom panel, black solid line). Our drift velocity calculated with Eq. (6) in the binary direction shows a maximum of $v_\perp = 770$ m/s at 3.0 K, whose value matches well with the second sound velocity $v = 780$ m/s measured in Ref. [10]. At variance with the experiment [10], we find, however, a dependence on the propagation direction (top panel, black solid and red dashed lines).

In conclusion, repopulation of phonon states by normal processes turns out to be particularly strong at low

temperatures and leads to the occurrence of the hydrodynamic regime in bismuth. We have shown that this effect is remarkably well accounted for in the exact solution of the BTE. This enables us to extract from the lattice thermal conductivity a characteristic length, the HWPL, whose behavior as a function of temperature, when compared to the phonon mean free path, is a fingerprint of the hydrodynamic-to-kinetic transition regime. Our calculated HWPL matches with macroscopic sample dimensions in which second sound was experimentally observed [10] and, together with Knudsen number and drift velocity, allow us to make the link with phonon hydrodynamics.

We acknowledge discussions with A. Cepellotti and A. McGaughey. Support from the DGA (France), the Chaire Énergie of the École Polytechnique, the program NEEDS-Matériaux (France), and from ANR-10-LABX-0039-PALM (Project Femtonic) is gratefully acknowledged. Computer time was granted by École Polytechnique through the LLR-LSI Project and by GENCI (Project No. 2210).

*maksim.markov@polytechnique.edu

[1] D. G. Cahill, P. V. Braun, G. Chen, D. R. Clarke, S. H. Fan, K. E. Goodson, P. Keblinski, W. P. King, G. D. Mahan, A. Majumdar *et al.*, Appl. Phys. Rev. **1**, 011305 (2014).
[2] S. Volz, J. Ordonez-Miranda, A. Shchepetov, M. Prunnila, J. Ahopelto, T. Pezeril, G. Vaudel, V. Gusev, P. Ruello, E. Weig *et al.*, Eur. Phys. J. B **89**, 15 (2016).
[3] C. W. Chang, D. Okawa, H. Garcia, A. Majumdar, and A. Zettl, Phys. Rev. Lett. **101**, 075903 (2008).
[4] N. Yand, G. Zhang, and B. Li, Nano Today **5**, 85 (2010).
[5] Y. Guo and M. Wang, Phys. Rep. **595**, 1 (2015).
[6] J. Zhang, X. Huang, Y. Yue, J. Wang, and X. Wang, Phys. Rev. B **84**, 235416 (2011).
[7] G. Fugallo, A. Cepellotti, L. Paulatto, M. Lazzeri, N. Marzari, and F. Mauri, Nano Lett. **14**, 6109 (2014).
[8] S. Lee, D. Broido, K. Esfarjani, and G. Chen, Nat. Commun. **6**, 6290 (2015).
[9] A. Cepellotti, G. Fugallo, L. Paulatto, M. Lazzeri, F. Mauri, and N. Marzari, Nat. Commun. **6**, 6400 (2015).
[10] V. Narayanamurti and R. Dynes, Phys. Rev. Lett. **28**, 1461 (1972).
[11] J.-P. Issi, Aust. J. Phys. **32**, 585 (1979).
[12] C. C. Ackerman, B. Bertman, H. A. Fairbank, and R. A. Guyer, Phys. Rev. Lett. **16**, 789 (1966).
[13] H. E. Jackson, C. T. Walker, and T. F. McNelly, Phys. Rev. Lett. **25**, 26 (1970).
[14] R. Guyer, Phys. Rev. E **50**, 4596 (1994).
[15] C. de Tomas, A. Cantarero, A. F. Lopeandia, and F. X. Alvarez, J. Appl. Phys. **115**, 164314 (2014).
[16] C. de Tomas, A. Cantarero, A. F. Lopeandia, and F. X. Alvarez, Proc. R. Soc. A **470**, 20140371 (2014).
[17] C. de Tomas, A. Cantarero, A. F. Lopeandia, and F. X. Alvarez, J. Appl. Phys. **118**, 134305 (2015).
[18] M. Omini and A. Sparavigna, Physica (Amsterdam) **212B**, 101 (1995).
[19] G. Fugallo, M. Lazzeri, L. Paulatto, and F. Mauri, Phys. Rev. B **88**, 045430 (2013).
[20] R. A. Guyer and J. A. Krumhansl, Phys. Rev. **148**, 778 (1966).
[21] See Supplemental Material at http://link.aps.org/supplemental/10.1103/PhysRevLett.120.075901 for detailed discussion, which includes Refs. [22,23].
[22] M. Park, I.-H. Lee, and Y.-S. Kim, J. Appl. Phys. **116**, 043514 (2014).
[23] A. Sparavigna, Phys. Rev. B **66**, 174301 (2002).
[24] R. Berman, E. Foster, and J. Ziman, Proc. R. Soc. A **231**, 130 (1955).
[25] A. Rajabpour, S. V. Allaei, Y. Chalopin, F. Kowsary, and S. Volz, J. Appl. Phys. **110**, 113529 (2011).
[26] O. Bourgeois, D. Tainoff, A. Tavakoli, Y. Liu, C. Blanc, M. Boukhari, A. Barski, and E. Hadji, C.R. Phys. **17**, 1154 (2016).
[27] M. Markov, J. Sjakste, G. Fugallo, L. Paulatto, M. Lazzeri, F. Mauri, and N. Vast, Phys. Rev. B **93**, 064301 (2016).
[28] M. Markov, Ph. D. thesis, Université Paris-Saclay, École Polytechnique (2016), https://pastel.archives-ouvertes.fr/tel-01438827.
[29] A. Sparavigna, Phys. Rev. B **65**, 064305 (2002).
[30] The longest dimension is along the binary direction. We used $L^{\mathrm{Cas}} = 2\sqrt{(l_1 l_2/\pi)}$ for this rectangular wire, whose experimental cross section is defined by the lengths l_1 and l_2. Choosing $L^{\mathrm{Cas}} = \sqrt{l_1 l_2} = 8.7$ mm has little effect on the scale of Fig. 1.
[31] C. Uher and H. J. Goldsmid, Phys. Status Solidi (b) **65**, 765 (1974).
[32] The longest dimension is along the trigonal axis. For the cross section, we have used a circular one oriented in (bisectrix, binary) plane with $L^{\mathrm{Cas}} = d$, where $d = 3.86$ mm is the experimental diameter of the cylindrical wire for sample 1. Choosing a spherical grain with $L^{\mathrm{Cas}} = 3.86$ mm would yield a minor difference in the temperature interval in which hydrodynamic phonon transport occurs.
[33] The longest dimension is along the binary axis. For the cross section, we have used a circular one oriented in (bisectrix, trigonal) plane with $L^{\mathrm{Cas}} = d$, where $d = 9.06$ mm is the experimental diameter of the cylindrical wire for sample 2. Choosing a spherical grain with $L^{\mathrm{Cas}} = 9.06$ mm would yield a minor difference in the temperature interval in which hydrodynamic phonon transport occurs.
[34] The idea of using LTC obtained with V-BTE to extract the phonon mean free paths was recently discussed in Ref. [35]. The method of Ref. [35] is different from our Eq. (7).
[35] V. Chiloyan, L. P. Zeng, S. Huberman, A. A. Maznev, K. A. Nelson, and G. Chen, Phys. Rev. B **93**, 155201 (2016).
[36] See Supplemental Material at http://link.aps.org/supplemental/10.1103/PhysRevLett.120.075901 for detailed discussion, which includes Refs. [37,38].
[37] A. Collaudin, Ph. D. thesis, Université Pierre et Marie CURIE Paris VI (2014).
[38] I. Y. Korenblit, M. E. Kuznetsov, V. M. Muzhdaba, and S. S. Shalyt, Sov. Phys. JETP **30**, 1009 (1970).
[39] R. Legrand, A. Huynh, B. Jusserand, B. Perrin, and A. Lemaitre, Phys. Rev. B **93**, 184304 (2016).